Earthquake Sequence Dynamics at the Interface Between an Elastic Layer and Underlying Half-Space in Antiplane Shear

Lauren S Abrahams[1], Kali L Allison[2], and Eric M Dunham[1]

[1]Stanford University
[2]University of Maryland

November 23, 2022

Abstract

We quantify sliding stability and rupture styles for a horizontal interface between an elastic layer and stiffer elastic half-space with a free surface on top and rate-and-state friction on the interface. This geometry includes shallowly dipping subduction zones, landslides, and ice streams. Specific motivation comes from quasi-periodic slow slip events on the Whillans Ice Plain in West Antarctica. We quantify the influence of layer thickness on sliding stability, specifically whether steady loading of the system produces steady sliding or sequences of stick-slip events. We do this using both linear stability analysis and nonlinear earthquake sequence simulations. We restrict our attention to the 2D antiplane shear problem, but anticipate that our findings generalize to the more complex 2D in-plane and 3D problems. Steady sliding with velocity-weakening rate-and-state friction is linearly unstable to Fourier mode perturbations having wavelengths greater than a critical wavelength (λ_c). We quantify the dependence of λ_c on the rate-and-state friction parameters, elastic properties, loading, and the layer thickness (H). We find that λ_c is proportional to sqrt(H) for small H and independent of H for large H. The linear stability analysis provides insight into nonlinear earthquake sequence dynamics of a nominally velocity-strengthening interface containing a velocity-weakening region of width W. Sequence simulations reveal a transition from steady sliding at small W to stick-slip events when W exceeds a critical width (W_cr), with W_cr proportional to sqrt(H) for small H. Overall this study demonstrates that the reduced stiffness of thin layers promotes instability, with implications for sliding dynamics in thin layer geometries.

Earthquake Sequence Dynamics at the Interface Between an Elastic Layer and Underlying Half-Space in Antiplane Shear

Lauren S. Abrahams[1], **Kali L. Allison**[2], **Eric M. Dunham**[1,3]

[1]Department of Geophysics, Stanford University, Stanford, CA, USA
[2]Department of Geology, University of Maryland, MD, USA
[3]Institute of Computational and Mathematical Engineering, Stanford University, Stanford, CA, USA

Key Points:

- We quantified sliding stability of an elastic layer over a stiffer half-space with rate-and-state friction at the interface
- Reduced stiffness of thin layers with a free surface on top promotes instability
- Conditions for slow slip sequences are explained by linear stability analysis

Corresponding author: Lauren S. Abrahams, `labraha2@stanford.edu`

Abstract

We quantify sliding stability and rupture styles for a horizontal interface between an elastic layer and stiffer elastic half-space with a free surface on top and rate-and-state friction on the interface. This geometry includes shallowly dipping subduction zones, landslides, and ice streams. Specific motivation comes from quasi-periodic slow slip events on the Whillans Ice Plain in West Antarctica. We quantify the influence of layer thickness on sliding stability, specifically whether steady loading of the system produces steady sliding or sequences of stick-slip events. We do this using both linear stability analysis and nonlinear earthquake sequence simulations. We restrict our attention to the 2D antiplane shear problem, but anticipate that our findings generalize to the more complex 2D in-plane and 3D problems.

Steady sliding with velocity-weakening rate-and-state friction is linearly unstable to Fourier mode perturbations having wavelengths greater than a critical wavelength (λ_c). We quantify the dependence of λ_c on the rate-and-state friction parameters, elastic properties, loading, and the layer thickness (H). We find that $\lambda_c \propto H^{1/2}$ for small H and independent of H for large H. The linear stability analysis provides insight into nonlinear earthquake sequence dynamics of a nominally velocity-strengthening interface containing a velocity-weakening region of width W. Sequence simulations reveal a transition from steady sliding at small W to stick-slip events when W exceeds a critical width (W_{cr}), with $W_{cr} \propto H^{1/2}$ for small H. Overall this study demonstrates that the reduced stiffness of thin layers promotes instability, with implications for sliding dynamics in thin layer geometries.

1 Introduction

Several geological hazards like earthquakes and landslides can be idealized as frictional sliding between two elastic solids. In response to steady loading, sliding can occur at either a steady rate or through stick-slip events. This sliding style is a function of the elastic properties of the solids, the geometry of the solids, the frictional parameters at the interface, and the loading. While most previous studies have focused on interfaces in otherwise unbounded solids, several systems and natural hazards involve sliding on interfaces close to a free surface. These include ice streams, shallowly dipping subduction zone faults, and landslides.

Ice streams are fast-moving rivers of ice that transport ice and debris from grounded ice sheets to the coast. Driven by gravity and/or push from comparatively steady upstream ice flow, ice streams involve sliding of a relatively thin (thickness $H \sim 1$ km) ice layer over nearly horizontal bedrock. Ice is an order of magnitude more compliant than bedrock, such that most deformation during slip occurs within the ice. While most ice streams slide in a relatively steady manner, the Whillians Ice Plain (WIP) in West Antarctica advances through twice-daily slow slip events. Each lasts about 30 minutes and causes about 0.5 m of slip with average rupture velocities of 100-300 m/s, an order of magnitude slower than the shear-wave speed of ice (Bindschadler et al., 2003; Walter et al., 2011). These stick-slip sequences are attributed to heterogeneity in the bed, specifically one or more "sticky-spots" of high frictional resistance (Alley, 1993; Winberry et al., 2011).

Likewise, shallowly dipping subduction zones, particularly the shallow region near the trench, involve sliding on an interface in close proximity and nearly parallel to the free surface. The hanging wall material above the interface is often vastly more compliant than the footwall material below the interface (Bilek & Lay, 1999; Polet & Kanamori, 2000; Jeppson et al., 2018), which influences rupture behavior and tsunamigenesis (Tanioka & Sataka, 1996; Kido et al., 2011; Kozdon & Dunham, 2013; Lotto et al., 2017; Sallarès & Ranero, 2019). Diverse sliding styles occur in the shallow subduction zone. These include steady aseismic sliding and slow slip (LaBonte et al., 2009; Wallace et al., 2016; Araki et al., 2017) that pose little hazard. Sliding can also occur in hazardous, tsunami-producing slip events, either as part of great megathrust ruptures (Simons et al., 2011; Lay et al., 2012) or as tsunami earthquakes (Pelayo & Wiens, 1992; Polet & Kanamori, 2000; Ma & Hirakawa, 2013) that are depleted in high-frequency seismic radiation relative to their magnitude. It is likely that elastic and frictional properties influence the sliding style, and that frictional properties are spatially heterogeneous (Lay & Kanamori, 1980, 1981).

Landslides also feature localized shearing on a slip surface with diverse sliding styles ranging from steady creep (Van Asch, 1984; Fruneau et al., 1996) to catastrophic shear failure (Gomberg et al., 1995; Hungr et al., 2014). Landslide models that explore slip stability are generally based on the idealization of frictional sliding on an interface close to the free surface (Palmer & Rice, 1973; Iverson, 2000; Viesca & Rice, 2012; Iverson & George, 2016; Handwerger et al., 2016). As in the other example systems, heterogeneity of material properties can lead to differences in the sliding style (Handwerger et al., 2016). The materials making up a landslide can significantly vary, leading to areas of high frictional resistance (rough surfaces with coarse-grained material) and lower frictional resistance (smooth surfaces with fine-grained liquefied material) (Baum & Johnson, 1993; Iverson, 2003).

In these three systems, an elastic layer slides across a nearly horizontal frictional interface, causing steady sliding or stick-slip sequences. A framework to explain these sliding styles has been developed through experiments to determine friction, theory to understand sliding stability, and simulations to explore nonlinear sliding dynamics.

Laboratory friction experiments have found that sliding between two solids can occur through either steady sliding and stick-slip motion reminiscent of earthquake ruptures (Brace & Byerlee, 1966; Dieterich, 1972, 1978). Stick-slip events have been further examined through rapid imaging in recent studies. These have shown more complex rupture styles, with stick-slip motion occurring as either slow slip events or inertially-controlled fast slip events (Rubinstein et al., 2004; Nielsen et al., 2010). Much earlier laboratory experiments led to the development of rate-and-state friction, a now well-established framework to describe friction at fault interfaces (Dieterich, 1978, 1979; Ruina, 1983; Rice & Ruina, 1983; Rice, 1983).

Rate-and-state friction plays a fundamental role in modern understanding of sliding stability. Rate-and-state friction describes the evolution of frictional strength with changes in slip velocity and sliding history. With an increase in slip velocity, there is a direct effect that initially increases the frictional resistance, then an evolution of frictional resistance to a new steady state value. This new steady state can feature either an increase in frictional resistance (velocity-strengthening) or a decrease in frictional resistance (velocity-weakening). In the context of rupture dynamics, a velocity-strengthening interface generally responds to steady loading through steady sliding. In contrast, sliding of a velocity-weakening interface can become unstable, producing earthquake-like slip events. Velocity-weakening interfaces are conditionally unstable; if frictional weakening happens more quickly than quasi-static stress reduction, then the interface will produce stick-slip events. For problem setups where the interface is completely velocity-weakening, the governing equations can be linearized around the steady state solution to quantify conditions for instability. Instability occurs if the perturbation wavelength is larger than a critical wavelength (λ_c), which is a function of the frictional parameters, elastic properties, loading, and material thickness. The stability of sliding between elastic solids has been studied in several contexts, including the study of elastic properties above and below the interface (identical vs. dissimilar materials) and the study of geometries (two half-spaces vs. layer over half-space) (Ruina, 1983; Rice et al., 2001; Ranjith, 2014; Aldam et al., 2016). A linear stability analysis can provide insight into more complex nonlinear frictional behavior that can only be studied with experiments or simulations.

Earthquake sequence simulations utilizing rate-and-state friction have been used to further examine instability and sliding dynamics. Several studies have been performed examining sliding between two half-spaces with a velocity-strengthening interface with a central velocity-weakening region. This frictional interface is the simplest idealization of real-world frictional heterogeneity. These studies have shown that a small velocity weakening region leads to aseismic slip (steady sliding), intermediate size leads to stick-slip sequences nucleating at the center of the velocity-weakening region, and very large velocity-weakening region leads to chaotic non-periodic rupture nucleated near the sides causing both partial and full ruptures (Sammis & Rice, 2001; Chen & Lapusta, 2009; Cattania & Segall, 2019; Barbot, 2019). The transition in size needed to cause instability (steady sliding to stick-slip sequences) is consistent with what is found in the linear stability analyses, with the onset of stick-slip cycles occurring when the velocity weakening zone is just larger than the nucleation length (Rubin & Ampuero, 2005; Ampuero & Rubin, 2008).

This study will focus on 2D antiplane shear sliding of a layer over half-space, which has been studied to a lesser extent (Ranjith, 2014; Bar-Sinai et al., 2013; Lipovsky & Dunham, 2017; Bar-Sinai et al., 2019). The linear stability analysis of this geometry can provide insight into earthquake sequences on more complex nonlinear interface frameworks, such as those of the WIP, shallowly dipping subduction zones, and landslides. Instability occurs when the velocity-weakening region is larger than some critical size. Therefore, we seek to quantify how instability depends on layer thickness, frictional parameters, elastic properties, and loading. First, we use a linear stability analysis to derive the critical wavelength for instability for an elastic layer over stiffer half-space with a velocity-weakening interface. Second, we justify that a compliant elastic layer over a stiffer underlying half-spaces, such as the ice-on-rock configuration of the WIP, can be treated as an elastic layer over a rigid half-space. Finally, we use numerical sequences simulations with a more complex distribution of frictional properties. We verify that key features of the linear stability analysis also describe sliding behavior for a more complex frictional interface.

2 Model and Governing Equations

Consider an elastic layer of thickness H sliding on a frictional interface over a half-space (Figure 1). In the linear stability analysis (section 3), the frictional interface is everywhere velocity-weakening (Figure 1a); instability occurs when a sinusoidal perturbation having wavelength (λ) larger than a critical wavelength (λ_c) is added to the steady sliding solution. In the numerical simulations (section 4), the frictional interface is velocity strengthening with a central velocity-weakening region (Figure 1b); stick-slip earthquake sequences occur in response to steady loading when the width (W) of the velocity-weakening region is larger than a critical width (W_{cr}). We demonstrate that the quantitative influence of H on sliding stability is consistent between the linear stability analysis and sequence simulations. For sufficiently small H, the critical length scales λ_c and W_{cr} both decrease as $H^{1/2}$ as H decreases. For large H, both critical length scales are independent of H.

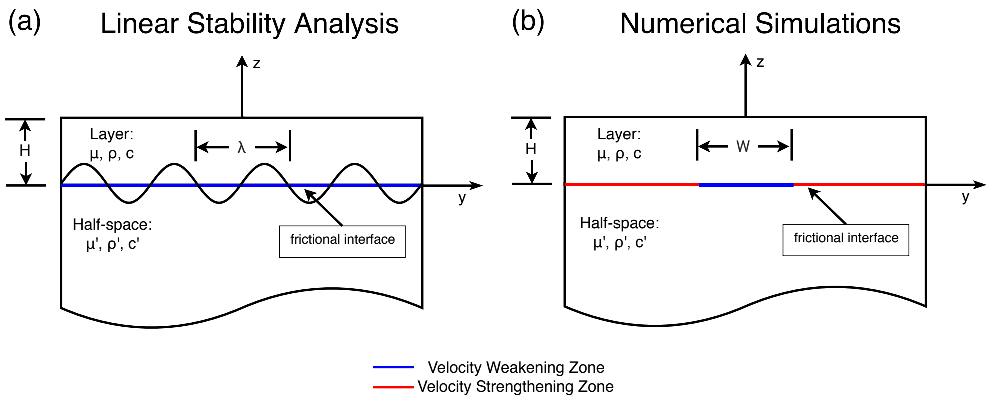

Figure 1. Antiplane shear sliding of an elastic layer over a half-space. (a) For the linear stability analysis, steady sliding on a velocity-weakening interface is unstable to sinusoidal perturbations having wavelengths (λ) larger than λ_c. (b) In the numerical simulations, the interface is velocity strengthening with a central region that is velocity-weakening. When the width of the region (W) is larger than W_{cr}, stick-slip sequences occur in response to steady forcing.

Three different slip styles (steady sliding, slow slip sequences, and fast slip sequences) can occur in the numerical simulations with steady forcing, with instability manifesting as the transition between steady sliding and slow slip sequences. Figure 2 shows three simulations, one for each slip style. (Simulation details are provided later.) The entire layer is sliding at a constant, steady state velocity at the start of the simulation. When $W < W_{cr}$, steady sliding occurs for the duration of the simulation (Figure 2, column 1). For W approximately equal to W_{cr}, perturbations about the steady state slip velocity grow and reach a limit cycle of slow slip events (Figure 2, column 2). When $W > W_{cr}$, fast slip event sequences occur (Figure 2, column 3). The transition from slow to fast slip is continuous and is distinguished by the relative of importance of inertia in the momentum balance. A primary objective of this study is to determine how layer thickness (H) influences W_{cr} and slip style.

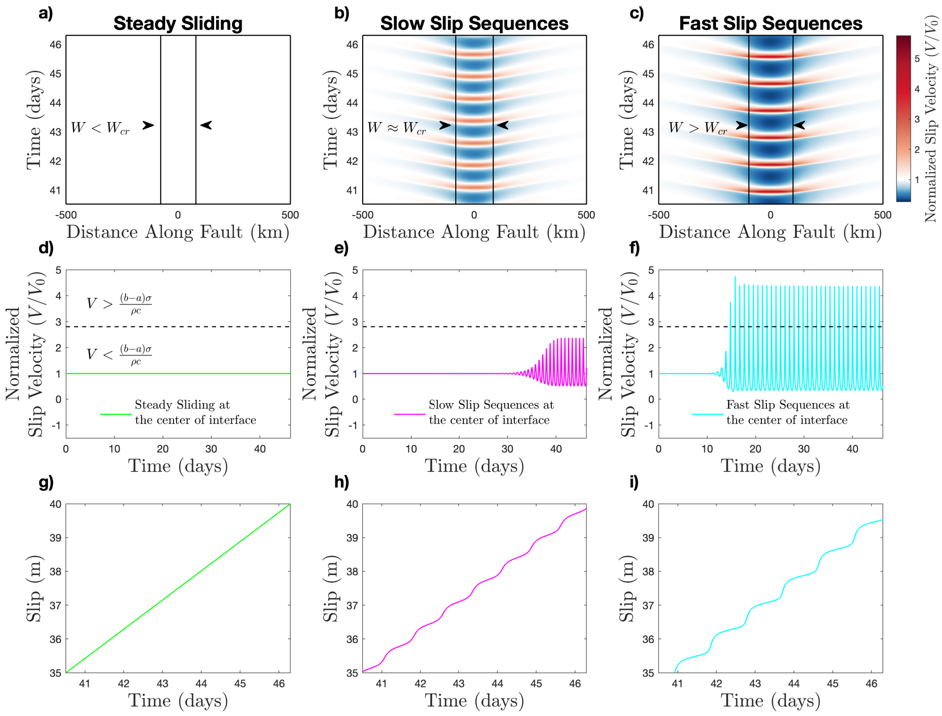

Figure 2. Simulation illustrating how increasing the width of the velocity-weakening region causes changes in sliding style style: column 1 (A, D, G) steady sliding; column 2 (B, E, H) slow slip events; column 3 (C, F, I) fast slip events. Row 1 (A, B, C): Space-time plots of normalized slip velocity. Row 2 (D, E, F): Normalized slip velocity at the center of the interface. Row 3 (G, H, I): Slip at the center of the interface.

2.1 Rate-and-state friction

Rate-and-state friction is a common framework to describe friction in tectonic settings (Dieterich, 1978, 1979, 1992; Ruina, 1983; Rice & Ruina, 1983; Marone, 1998; Rice et al., 2001). Frictional strength (τ) at the interface is a function of sliding velocity (V), a state variable that quantifies sliding history (θ), and effective normal stress (σ):

$$\tau = f(V, \theta)\sigma, \tag{1}$$

with friction coefficient

$$f(V, \theta) = f_0 + a \ln\left(\frac{V}{V_0}\right) + b \ln\left(\frac{V_0 \theta}{d_c}\right), \tag{2}$$

where f_0 and V_0 are reference friction coefficient and reference sliding velocity, a and b are rate-and-state coefficients, and d_c is the state evolution distance. We use the aging law for state evolution:

$$\frac{\partial \theta}{\partial t} = 1 - \frac{\theta V}{d_c}. \tag{3}$$

At steady state $\partial\theta/\partial t = 0$, for which state assumes its steady state value $\theta_{ss}(V) = d_c/V$. Substituting this into the friction law (1) and (2) provides the steady state frictional strength,

$$\tau_{ss}(V) = \sigma\left[f_0 + (a-b)\ln\left(\frac{V}{V_0}\right)\right]. \tag{4}$$

When $a - b > 0$ friction is velocity strengthening, corresponding to steady sliding in response to steady forcing, whereas when $a-b < 0$ friction is velocity-weakening which can lead to unstable slip and earthquake sequences (Rice & Ruina, 1983; Rice, 1983). Keeping σ constant and linearizing the frictional strength (1) and (2) about a steady state velocity (V_0) yields (Rice, 1983; Rice et al., 2001):

$$\frac{\partial\tau}{\partial t} = \frac{a\sigma}{V_0}\frac{\partial V}{\partial t} - \frac{V_0}{d_c}\left((\tau-\tau_0) + \frac{\sigma(b-a)}{V_0}(V-V_0)\right), \tag{5}$$

where $\tau_0 = \tau_{ss}(V_0)$ and, without loss of generality, the reference velocity to equal steady state velocity. We will utilize (5) in the linear stability analysis to follow.

2.2 Elasticity and loading

In the 2D antiplane shear model setup, there is an elastic layer above the interface ($z > 0$) and an elastic half-space below the interface ($z < 0$). The materials above and below the interface are possibly different (shear moduli μ and μ', density ρ and ρ', which together give shear wave speeds $c = \sqrt{\mu/\rho}$ and $c' = \sqrt{\mu'/\rho'}$), with the prime indicating material properties in the half-space. In the numerical simulations, we take the half-space to be rigid ($\mu' \to \infty$ and $c' \to \infty$). The layer slides in the x-direction relative to the half-space, with the y-direction along the interface and the z-direction upward (Figure 1). There is a spatially uniform effective normal stress (σ) along the interface at $z = 0$.

In this study, which focuses primarily on the transition between steady sliding and slow slip, we solve the quasi-static elastic problem and, in numerical simulations only (but not in the linear stability analysis), utilize the radiation damping approximation to capture inertial effects. Quasi-static stresses are denoted as σ_{ij}. The top of the layer, at $z = H$, is traction free,

$$\sigma_{xz}(y, z = H, t) = 0. \tag{6}$$

For antiplane shear sliding, displacement occurs in the x-direction only; therefore, $u_y = u_z = 0$ and we define $u = u_x(y, z, t)$. The slip across the interface is

$$\delta(y,t) = u(y, z = 0^+, t) - u(y, z = 0^-, t), \tag{7}$$

and slip velocity is $V(y,t) = \partial\delta/\partial t$. Shear tractions are balanced across the interface,

$$\sigma_{xz}(y, z = 0^-, t) = \sigma_{xz}(y, z = 0^+, t). \tag{8}$$

At the interface, the shear stress is the sum of the quasi-static shear stress and the radiation damping stress change (Rice, 1993),

$$\tau(y,t) = \sigma_{xz}(y, z = 0, t) - \eta V, \tag{9}$$

where the radiation damping term is neglected (i.e., $\eta = 0$) in the linear stability analysis whereas $\eta = \mu/c$ in the numerical simulations. Hooke's law,

$$\sigma_{xy} = \mu\frac{\partial u}{\partial y} \quad \text{and} \quad \sigma_{xz} = \mu\frac{\partial u}{\partial z}, \tag{10}$$

relates stress and elastic strain, where μ differs above and below the interface.

The layer slides due to an applied body force (f_x) applied only in the layer, making the 2D equilibrium equations

$$0 = \mu \left(\frac{\partial^2 u}{\partial y^2} + \frac{\partial^2 u}{\partial z^2} \right) + f_x \tag{11}$$

above the interface ($z > 0$) and

$$0 = \mu' \left(\frac{\partial^2 u}{\partial y^2} + \frac{\partial^2 u}{\partial z^2} \right) \tag{12}$$

below the interface ($z < 0$).

Fast slip events are defined as those for which inertial effects, appearing through the $-\eta V$ term, are appreciable. We use the following criterion to distinguish fast from slow slip, but note that the transition is gradual:

$$V > \frac{(b-a)\sigma}{\mu} c. \tag{13}$$

The body force causes the layer to slide at a steady state velocity V_0 in the absence of perturbations. Using the equation of motion (11), we can obtain the forcing term (f_x) by integrating the equilibrium equation (11) over the domain, utilizing the free surface boundary condition (6), and setting shear stress on the interface (9) equal to frictional strength (1). For spatially uniform forcing and sliding in steady state conditions, we find

$$f_x = \frac{\tau_{ss}(V_0) - \eta V_0}{H}. \tag{14}$$

2.3 Parameter choices

The setup of a velocity-weakening region within a velocity-strengthening interface that we use in our simulations (Figure 1b) is motivated by the Whillans Ice Plain (WIP). This section of an Antarctic ice stream exhibits twice-daily slow slip events (Walter et al., 2011). Because of our interest in this phenomenon, we base our nominal model parameters on those of ice (Table 1). However, we note that the model setup and analysis results apply to a wide range of elastic properties and frictional parameters, such as shallowly dipping subduction zones and landslides. Therefore, the results of this study are normalized to encompass various types of geologic settings.

Table 1. Parameters used in the linearized stability analysis and numerical simulations. Model parameters based on those of ice.

Symbol	Parameter	Value
f_0	reference friction coefficient	0.4
V_0	reference velocity (and steady state velocity)	10^{-5} m/s
d_c	state evolution distance	0.014 m
σ	effective normal stress	101 kPa
a	direct effect parameter	0.02
b_{VS}	evolution effect parameter for velocity-strengthening region	0.015
b_{VW}	evolution effect parameter for velocity-weakening region	0.025
μ	layer shear modulus	3.6 GPa
ρ	layer density	900 kg/m^3
η	radiation damping coefficient	1.8 MPa/(m/s)

3 Linear Stability Analysis

For a velocity-weakening interface subject to constant loading, sliding occurs at a steady velocity in the absence of perturbations. When the system is perturbed, the perturbation can grow to cause instability or decay to return the system to its steady sliding state. Steady sliding on a velocity-weakening interface (Figure 1a) is linearly unstable to Fourier mode perturbations having wavelengths greater than the critical wavelength (λ_c). This critical wavelength is dependent on layer thickness (H), the elastic properties, and the rate-and-state parameters. We examine a perturbation added to steady state in slip ($\hat{\delta}$), slip velocity ($\hat{V}$), and shear stress ($\hat{\tau}$) to quantify the response. This perturbation is of the form $\exp(iky+pt)$, where $k = 2\pi/\lambda$ is a real wavenumber and $p = \zeta + i\omega$ is complex and characterizes the time response to the perturbation as a function of k. For quasi-static elasticity (without radiation damping), the perturbations are

$$\hat{\delta} = \delta - V_0 t = D(k,p)e^{iky+pt}, \tag{15}$$

$$\hat{V} = V - V_0 = p\hat{\delta}, \tag{16}$$

and

$$\hat{\tau} = \tau - \tau_0 = T(k,p)\hat{\delta}, \tag{17}$$

where $D(k,p)$ is the amplitude of the perturbation and

$$T(k,p) = -\frac{\mu' \mu |k|}{\mu + \mu' \coth(|k|H)}, \tag{18}$$

as derived in Ranjith (2014) by solving the quasi-static elasticity problem stated in Section 2.2. Without loss of generality we choose reference velocity to be equal to steady state velocity denoted as V_0 and $\tau_0 = \tau_{ss}(V_0)$. For these Fourier mode perturbations, the linearized friction law (5) becomes

$$\hat{\tau}\left(p + \frac{V_0}{d_c}\right) = \frac{\sigma}{V_0}\left(ap - (b-a)\frac{V_0}{d_c}\right)p\hat{\delta}. \tag{19}$$

Substituting the elasticity relation (17) into (19) and defining $\epsilon = \mu/\mu'$ as the shear moduli ratio, we obtain the characteristic equation

$$\left(p + \frac{V_0}{d_c}\right)\frac{-\mu|k|}{\epsilon + \coth(|k|H)} = \frac{\sigma}{V_0}\left(ap - (b-a)\frac{V_0}{d_c}\right)p. \tag{20}$$

This is a quadratic equation for p that has two solutions.

Note first that when $k \to \infty$, the solutions p are real and negative, causing short wavelength perturbations to be damped and the system to return to steady sliding. Second, $p = 0$ is not a solution to the characteristic equation for $k > 0$.

We next focus on conditions for neutral stability, i.e., $\zeta = \Re(p) = 0$. Separating the real and imaginary parts of the characteristic equation (20) and setting $\zeta = 0$, we obtain the following neutral stability condition:

$$\frac{\mu k_c}{\epsilon + \coth(k_c H)} = \frac{\sigma(b-a)}{d_c}, \tag{21}$$

where we have denoted the solution k as the critical wavenumber k_c; the corresponding critical wavelength is $\lambda_c = 2\pi/k_c$. Numerical solutions to (21) are shown in Figure 3 with normalization described below.

3.1 Linear stability analysis – Limits

Multiple limits, including limits in layer thickness relative to perturbation wavelength (kH) and material properties ($\epsilon = \mu/\mu'$), can be examined for the neutral stability condition (21). If we consider the overlying layer as a half-space ($H \to \infty$), (21) has the solution

$$k_c = (\epsilon + 1)\frac{\sigma(b-a)}{\mu d_c}. \tag{22}$$

When $\epsilon = 1$, this solution reaches the well-known neutral stability condition for a frictional interface in a homogeneous elastic whole-space (Rice & Ruina, 1983; Rice et al., 2001),

$$k_c = \frac{2\sigma(b-a)}{\mu d_c}. \tag{23}$$

When the half-space above the interface is elastic and the half-space below the interface is rigid, $\epsilon \to 0$ and the critical wavelength becomes

$$\lambda_\infty = \frac{2\pi\mu d_c}{\sigma(b-a)}. \tag{24}$$

This solution is used to normalize length scales in Figures 3 and 4, and is shown as the red dashed line in Figure 3a.

Next, if we consider the overlying layer as being small relative to the perturbation wavelength ($|k|H \ll 1$), the neutral stability condition (21) reduces to

$$\frac{\mu H k_c^2}{\epsilon H k_c + 1} = \frac{\sigma(b-a)}{d_c}, \tag{25}$$

and the critical wavenumber is

$$k_c = \frac{\epsilon\sigma(b-a)}{2\mu d_c} + \sqrt{\left[\frac{\epsilon\sigma(b-a)}{2\mu d_c}\right]^2 + \frac{\sigma(b-a)}{H\mu d_c}}. \tag{26}$$

If, in addition, the half-space below the interface is rigid ($\epsilon \to 0$), the critical wavelength is

$$\lambda_{thin} = 2\pi\sqrt{\frac{H\mu d_c}{\sigma(b-a)}}. \tag{27}$$

This limit was examined by Lipovsky and Dunham (2017) in their study of the Whillans Ice Plain stick-slip events, and appears as the black dashed line in Figure 3a. From Figure 3a, we see that the critical wavelength transitions continuously from the thin layer limit (27) to the half-space limit (24) as layer thickness increases.

Figure 3b displays critical wavelengths for different choices of material properties ($\epsilon = \mu/\mu'$). When $\epsilon = 1$, the layer and half-space have identical material properties. When $\epsilon = 0$, the underlying half-space is rigid. At small layer thicknesses, the critical wavelengths converge for all ϵ values—showing that in this limit the shear modulus of the half-space becomes irrelevant. For larger layer thicknesses, the critical wavelength becomes independent of layer thickness, but does depend on ϵ.

For the earthquake sequence simulations (Section 4), we assume the underlying half-space to be rigid ($\epsilon = 0$). These simulations are specifically motivated by the WIP stick-slip events that involve sliding of ice over rock, for which we estimate $\epsilon = 0.111$. To quantify when the rigid half-space approximation is valid, we examine dependence on ϵ for two limits: the half-space over a half-space limit and the thin layer over a half-space limit. For the half-space over half-space limit ($H \to \infty$), examining (22) shows that the error between using ice/rock properties ($\epsilon = 0.111$) and ice/rigid properties ($\epsilon = 0$) is only 11%. For the thin layer limit ($|k|H \ll 1$) that is arguably more relevant to the WIP, Taylor series expansion of (26) in ϵ about $\epsilon = 0$ gives

$$k_c = \sqrt{\frac{\sigma(b-a)}{H\mu d_c}}\left(1 + \epsilon\sqrt{\frac{\sigma(b-a)H}{4\mu d_c}}\right) + \mathcal{O}(\epsilon^2). \tag{28}$$

This shows that the elastic properties of the underlying half-space do not significantly affect the solution. This is seen in Figure 3b, which shows that the critical wavelength

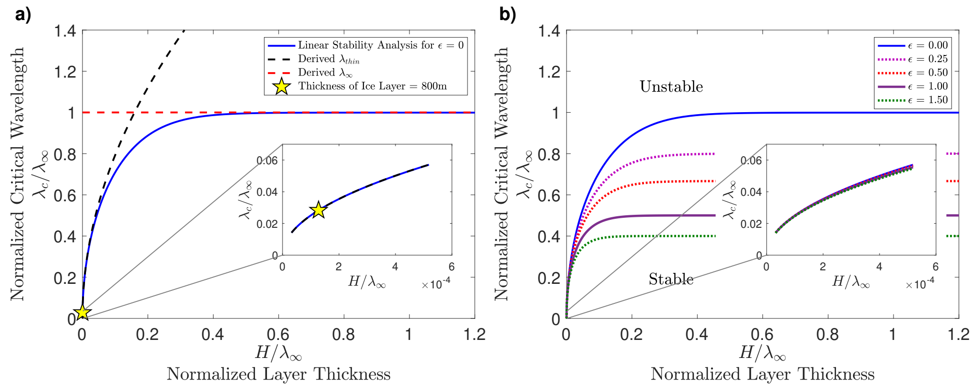

Figure 3. (a) Critical wavelength for an elastic layer over rigid half-space ($\epsilon = 0$). The critical wavelength asymptotes to λ_{thin}, equation (27), when $H/\lambda_\infty \ll 1$ and λ_∞, equation (24), when $H/\lambda_\infty \gg 1$. (b) Dependence of critical wavelength on shear moduli ratio ϵ. Note convergence of critical wavelengths for $H/\lambda_\infty \ll 1$. Only the shear modulus of the layer is relevant in this limit.

becomes independent of ϵ for $H/\lambda_\infty \ll 1$. Therefore, we conclude that if the half-space below the interface is significantly stiffer than the layer above, the underlying half-space can be modeled as rigid.

In the next section, we turn to earthquake sequence simulations to explore nonlinear slip dynamics, with a similar problem set up involving sliding of a layer over half-space, but with a velocity-weakening region in an otherwise velocity-strengthening interface (Figure 1). Although this problem setup is somewhat different than the linear stability analysis, we anticipate similar dependence on layer height, elastic properties, and frictional parameters. Specifically, we found from the linear stability analysis that for large H, the critical wavelength becomes independent of the layer thickness. Likewise, for small H, the critical wavelength becomes proportional to $H^{1/2}$. We hypothesize that similar dependence on H will appear for the critical width (W_{cr}) of the velocity-weakening region that delimits the transition between steady sliding and slow slip sequences.

4 Earthquake sequence simulations

In this section we consider earthquake sequence simulations for an elastic layer sliding on a rigid half-space. The interface has a velocity-weakening region of width W in an otherwise velocity-strengthening interface (Figure 1b). Our objective is to determine the critical width (W_{cr}) that marks the boundary between steady sliding and stick-slip event sequences. Three different styles of slip can occur: steady sliding, slow slip sequences, and fast slip sequences (Figure 2). We predict that the transition between steady sliding and slow slip sequences will have a similar dependence on layer thickness to the linear stability analysis.

4.1 Simulation framework

We briefly supplement the model description from Section 2 with a few implementation details. The computational domain is truncated in the y-direction with traction-free boundary conditions that permit continued slip without development of elastic strains,

$$\sigma_{xy}\left(\pm\frac{L_y}{2}, z, t\right) = 0. \tag{29}$$

The domain boundaries are placed sufficiently far from the velocity-weakening region that there is negligible effect on the earthquake sequences. Specifically, the size of the domain in the y-direction (L_y) is 60 times larger than the critical wavelength (λ_c) calculated in the linear stability analysis. At the edge of the domain, slip velocity fluctuates by $< 0.001\%$ about the steady state velocity. The velocity-weakening region is well resolved, with a constant grid spacing of $\lambda_c/160$ for $|y| < 2\lambda_c$. Outside this region, the grid spacing increases continuously following a cubic function that passes through $\lambda_c/80$ at $|y| = 3\lambda_c$ and $\lambda_c/4$ at $|y| = 10\lambda_c$.

At the start of the simulation, the frictional resistance (4) is uniform along the interface (regardless of whether that section of the interface is velocity-strengthening or velocity-weakening because steady state velocity and the reference velocity are equal). Simulations are run for sufficiently long time that results become independent of initial conditions. We observe that if the width of the velocity-weakening region (W) is larger than a critical width (W_{cr}), perturbations about steady sliding (arising from numerical error) grow until the system reaches a limit cycle of slow or fast slip sequences (Figure 2 E, F).

We classify slip style as a function of W as follows, noting that the transitions between slip styles are continuous so the delimiting criteria are somewhat arbitrary. We define the onset of slow slip sequences (Figure 2, column 2) when slip velocity perturbations first exceed $V/V_0 = 1.1$. The transition from slow slip sequences to fast slip sequences (Figure 2, column 3) is determined by the importance of inertia as quantified by (13). For our model parameters, this corresponds to $V/V_0 = 2.8$.

4.2 Simulation results

We perform earthquake sequence simulations for a variety of H and W values and classify slip style using the criteria defined above. Figure 4 shows the resulting parameter space study. Also shown in Figure 4 is the linear stability analysis prediction of critical wavelength λ_c as a function of H. While the critical wavelength prediction does not exactly match the boundary between steady sliding and slow slip events, there is remarkable similarity in the dependence on H. Specifically, we find that W_{cr} increases as $H^{1/2}$ for $H/\lambda_\infty \ll 1$ and becomes independent of H for $H/\lambda_\infty \gg 1$. However, we do note some quantitative differences, such as the discrepancy between the asymptotic values of λ_c and W_{cr} for large layer thicknesses. This discrepancy is most likely due to the difference in the frictional property distribution between the linear stability analysis (uniformly velocity-weakening) and sequence simulations (velocity-weakening region in velocity-strengthening interface). Earthquake sequence simulations have a more complex frictional interface compared to the linear stability analysis. Thus we do not expect an exact correspondence between the linear stability analysis and numerical sequence simulation. Nonetheless, we do conclude that the proximity of the free surface in the thin layer limit influences slip behavior in the same manner in the sequence simulations as in the linear stability analysis.

5 Conclusions

In this study we examined the sliding dynamics of a frictional interface between elastic solids. The motivation of this work was to quantify sliding stability and slip styles for a layer over half-space geometry with a free surface on top and rate-and-state friction at the interface. To understand the effects of layer thickness (H), we performed a linear stability analysis and earthquake sequence simulations. In the linear stability analysis, we quantified dependence of the critical wavelength on layer thickness and the ratio of shear moduli above and below the interface. We justified conditions for which the underlying half-space can be regarded as rigid, and showed that this rigid half-space approximation is well justified for ice sliding on rock. The earthquake sequence simulations,

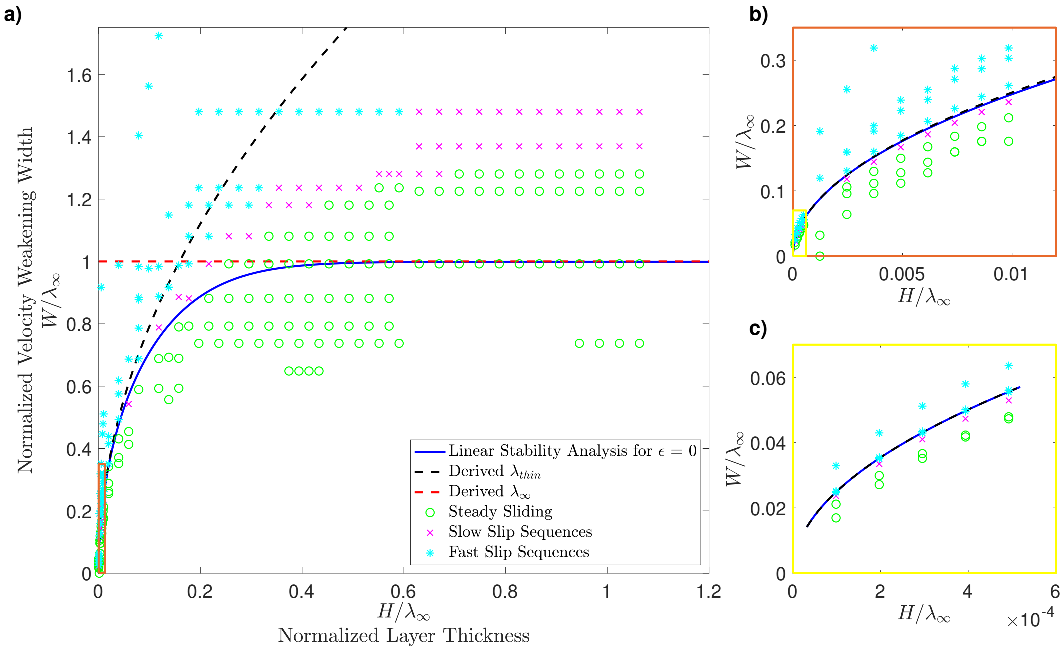

Figure 4. Dependence of slip style (steady sliding, slow slip events, and fast slip events) on width of velocity-weakening region (W) and layer thickness (H). Also shown is the linear stability analysis prediction (for which the W/λ_∞ axis should be interpreted as λ_c/λ_∞). For both the linear stability analysis and numerical sequences simulation for small layer thickness, H/λ_∞, the critical instability length is proportional to $H^{1/2}$, emphasized in b and c. For large H/λ_∞, the critical instability length becomes independent of H.

featuring a velocity-weakening region in an otherwise velocity-strengthening interface, were conducted using this approximation. We found that the critical width of the velocity-weakening region, which marks the transition between steady sliding and slow slip events, depends on layer thickness (H) as $H^{1/2}$ for sufficiently small H. This is exactly the same dependence that was revealed by the linear stability analysis. In particular, we note that the critical width or wavelength can be vastly smaller in this thin layer limit than when the layer thickness is large, as compared to the critical stability length in the thick-layer limit. This finding demonstrates the importance of accounting for free surface effects in problems involving frictional sliding on surfaces that are subparallel to and in close proximity to the free surface. Such sliding problems arise in the context of ice streams, the shallow region of subduction zones, and landslides. Of course, each of these problems features additional complexities, such as viscoelasticity and thermomechanical effects for the ice stream problem, and fluids in likely all cases, that must be considered for a proper characterization of the system. Furthermore, we have limited attention to the simplest 2D antiplane shear problem, whereas the 2D in-plane and fully 3D problems would also feature normal stress changes due to elastic and geometrical mismatch across the interface. These are all potential topics for additional work. Nonetheless, this study demonstrates how the decreasing elastic stiffness associated with small layer thickness reduces the critical length for instability, with important implications for rupture dynamics in thin layer geometries.

Acknowledgments

This material is based upon work supported by the National Science Foundation Graduate Research Fellowship under Grant No. DGE - 1656518. Additional support from Stanford's Enhancing Diversity in Graduate Education (EDGE) Doctoral Fellowship Program.

Numerical earthquake sequences simulations were performed through the 2D earthquake cycle code SCycle (https://bitbucket.org/kallison/scycle/src/master/). Representative input files are available through the U.S. Antarctic Program Data Center DOI 10.15784/601320 (https://www.usap-dc.org/view/dataset/601320).

References

Aldam, M., Bar-Sinai, Y., Svetlizky, I., Brener, E. A., Fineberg, J., & Bouchbinder, E. (2016). Frictional sliding without geometrical reflection symmetry. *Physical Review X*, *6*(4), 041023.

Alley, R. B. (1993). In search of ice-stream sticky spots. *Journal of Glaciology*, *39*(133), 447–454.

Ampuero, J.-P., & Rubin, A. M. (2008). Earthquake nucleation on rate and state faults–aging and slip laws. *Journal of Geophysical Research: Solid Earth*, *113*(B1).

Araki, E., Saffer, D. M., Kopf, A. J., Wallace, L. M., Kimura, T., Machida, Y., ... others (2017). Recurring and triggered slow-slip events near the trench at the nankai trough subduction megathrust. *Science*, *356*(6343), 1157–1160.

Barbot, S. (2019). Slow-slip, slow earthquakes, period-two cycles, full and partial ruptures, and deterministic chaos in a single asperity fault. *Tectonophysics*, *768*, 228171.

Bar-Sinai, Y., Aldam, M., Spatschek, R., Brener, E. A., & Bouchbinder, E. (2019). Spatiotemporal dynamics of frictional systems: The interplay of interfacial friction and bulk elasticity. *Lubricants*, *7*(10), 91.

Bar-Sinai, Y., Spatschek, R., Brener, E. A., & Bouchbinder, E. (2013). Instabilities at frictional interfaces: Creep patches, nucleation, and rupture fronts. *Physical Review E*, *88*(6), 060403.

Baum, R. L., & Johnson, A. M. (1993). *Steady movement of landslides in fine-grained soils: A model for sliding over an irregular slip surface* (No. 1842). US Government Printing Office.

Bilek, S. L., & Lay, T. (1999). Rigidity variations with depth along interplate megathrust faults in subduction zones. *Nature*, *400*(6743), 443–446.

Bindschadler, R. A., Vornberger, P. L., King, M. A., & Padman, L. (2003). Tidally driven stick–slip motion in the mouth of whillans ice stream, antarctica. *Annals of Glaciology*, *36*, 263–272.

Brace, W., & Byerlee, J. (1966). Stick-slip as a mechanism for earthquakes. *Science*, *153*(3739), 990–992.

Cattania, C., & Segall, P. (2019). Crack models of repeating earthquakes predict observed moment-recurrence scaling. *Journal of Geophysical Research: Solid Earth*, *124*(1), 476–503.

Chen, T., & Lapusta, N. (2009). Scaling of small repeating earthquakes explained by interaction of seismic and aseismic slip in a rate and state fault model. *Journal of Geophysical Research: Solid Earth*, *114*(B1).

Dieterich, J. H. (1972). Time-dependent friction in rocks. *Journal of Geophysical Research*, *77*(20), 3690–3697.

Dieterich, J. H. (1978). Time-dependent friction and the mechanics of stick-slip. In *Rock friction and earthquake prediction* (pp. 790–806). Springer.

Dieterich, J. H. (1979). Modeling of rock friction: 1. experimental results and constitutive equations. *Journal of Geophysical Research: Solid Earth*, *84*(B5), 2161–2168.

Dieterich, J. H. (1992). Earthquake nucleation on faults with rate-and state-dependent strength. *Tectonophysics*, *211*(1-4), 115–134.

Fruneau, B., Achache, J., & Delacourt, C. (1996). Observation and modelling of the saint-etienne-de-tinée landslide using sar interferometry. *Tectonophysics*, *265*(3-4), 181–190.

Gomberg, J., Bodin, P., Savage, W., & Jackson, M. E. (1995). Landslide faults and tectonic faults, analogs?: The slumgullion earthflow, colorado. *Geology*, *23*(1), 41–44.

Handwerger, A. L., Rempel, A. W., Skarbek, R. M., Roering, J. J., & Hilley, G. E. (2016). Rate-weakening friction characterizes both slow sliding and catastrophic failure of landslides. *Proceedings of the National Academy of Sciences*, *113*(37), 10281–10286.

Hungr, O., Leroueil, S., & Picarelli, L. (2014). The varnes classification of landslide types, an update. *Landslides*, *11*(2), 167–194.

Iverson, R. M. (2000). Landslide triggering by rain infiltration. *Water resources research*, *36*(7), 1897–1910.

Iverson, R. M. (2003). The debris-flow rheology myth. *Debris-flow hazards mitigation: mechanics, prediction, and assessment*, *1*, 303–314.

Iverson, R. M., & George, D. L. (2016). Modelling landslide liquefaction, mobility bifurcation and the dynamics of the 2014 oso disaster. *Géotechnique*, *66*(3), 175–187.

Jeppson, T. N., Tobin, H. J., & Hashimoto, Y. (2018). Laboratory measurements quantifying elastic properties of accretionary wedge sediments: Implications for slip to the trench during the 2011 m w 9.0 tohoku-oki earthquake. *Geosphere*, *14*(4), 1411–1424.

Kido, M., Osada, Y., Fujimoto, H., Hino, R., & Ito, Y. (2011). Trench-normal variation in observed seafloor displacements associated with the 2011 tohoku-oki earthquake. *Geophysical Research Letters*, *38*(24).

Kozdon, J. E., & Dunham, E. M. (2013). Rupture to the trench: Dynamic rupture simulations of the 11 march 2011 tohoku earthquake. *Bulletin of the Seismological Society of America*, *103*(2B), 1275–1289.

LaBonte, A. L., Brown, K. M., & Fialko, Y. (2009). Hydrologic detection and finite element modeling of a slow slip event in the costa rica prism toe. *Journal of Geophysical Research: Solid Earth*, *114*(B4).

Lay, T., & Kanamori, H. (1980). Earthquake doublets in the solomon islands. *Physics of the Earth and Planetary Interiors*, *21*(4), 283–304.

Lay, T., & Kanamori, H. (1981). An asperity model of large earthquake sequences.

Lay, T., Kanamori, H., Ammon, C. J., Koper, K. D., Hutko, A. R., Ye, L., ... Rushing, T. M. (2012). Depth-varying rupture properties of subduction zone megathrust faults. *Journal of Geophysical Research: Solid Earth*, *117*(B4).

Lipovsky, B. P., & Dunham, E. M. (2017). Slow-slip events on the Whillans Ice Plain, Antarctica, described using rate-and-state friction as an ice stream sliding law. *Journal of Geophysical Research: Earth Surface*, *122*(4), 973–1003.

Lotto, G. C., Dunham, E. M., Jeppson, T. N., & Tobin, H. J. (2017). The effect of compliant prisms on subduction zone earthquakes and tsunamis. *Earth and Planetary Science Letters*, *458*, 213–222.

Ma, S., & Hirakawa, E. T. (2013). Dynamic wedge failure reveals anomalous energy radiation of shallow subduction earthquakes. *Earth and Planetary Science Letters*, *375*, 113–122.

Marone, C. (1998). Laboratory-derived friction laws and their application to seismic faulting. *Annual Review of Earth and Planetary Sciences*, *26*(1), 643–696.

Nielsen, S., Taddeucci, J., & Vinciguerra, S. (2010). Experimental observation of stick-slip instability fronts. *Geophysical Journal International*, *180*(2), 697–702.

Palmer, A. C., & Rice, J. R. (1973). The growth of slip surfaces in the progressive failure of over-consolidated clay. *Proceedings of the Royal Society of London. A. Mathematical and Physical Sciences*, *332*(1591), 527–548.

Pelayo, A. M., & Wiens, D. A. (1992). Tsunami earthquakes: Slow thrust-faulting events in the accretionary wedge. *Journal of Geophysical Research: Solid Earth*, *97*(B11), 15321–15337.

Polet, J., & Kanamori, H. (2000). Shallow subduction zone earthquakes and their tsunamigenic potential. *Geophysical Journal International*, *142*(3), 684–702.

Ranjith, K. (2014). Instabilities in dynamic anti-plane sliding of an elastic layer on a dissimilar elastic half-space. *Journal of Elasticity*, *115*(1), 47–59.

Rice, J. R. (1983). Constitutive relations for fault slip and earthquake instabilities. In *Instabilities in continuous media* (pp. 443–475). Springer.

Rice, J. R. (1993). Spatio-temporal complexity of slip on a fault. *Journal of Geophysical Research: Solid Earth*, *98*(B6), 9885–9907.

Rice, J. R., Lapusta, N., & Ranjith, K. (2001). Rate and state dependent friction and the stability of sliding between elastically deformable solids. *Journal of the Mechanics and Physics of Solids*, *49*(9), 1865–1898.

Rice, J. R., & Ruina, A. L. (1983). Stability of steady frictional slipping. *Journal of applied mechanics*, *50*(2), 343–349.

Rubin, A. M., & Ampuero, J.-P. (2005). Earthquake nucleation on (aging) rate and state faults. *Journal of Geophysical Research: Solid Earth*, *110*(B11).

Rubinstein, S. M., Cohen, G., & Fineberg, J. (2004). Detachment fronts and the onset of dynamic friction. *Nature*, *430*(7003), 1005–1009.

Ruina, A. L. (1983). Slip instability and state variable friction laws. *Journal of Geophysical Research: Solid Earth*, *88*(B12), 10359–10370.

Sallarès, V., & Ranero, C. R. (2019). Upper-plate rigidity determines depth-varying rupture behaviour of megathrust earthquakes. *Nature*, *576*(7785), 96–101.

Sammis, C. G., & Rice, J. R. (2001). Repeating earthquakes as low-stress-drop events at a border between locked and creeping fault patches. *Bulletin of the Seismological Society of America*, *91*(3), 532–537.

Simons, M., Minson, S. E., Sladen, A., Ortega, F., Jiang, J., Owen, S. E., … others (2011). The 2011 magnitude 9.0 tohoku-oki earthquake: Mosaicking the megathrust from seconds to centuries. *science*, *332*(6036), 1421–1425.

Tanioka, Y., & Sataka, K. (1996). Fault parameters of the 1896 sanriku tsunami earthquake estimated from tsunami numerical modeling. *Geophysical Research Letters*, *23*(13), 1549–1552.

Van Asch, T. W. (1984). Creep processes in landslides. *Earth Surface Processes and Landforms*, *9*(6), 573–583.

Viesca, R. C., & Rice, J. R. (2012). Nucleation of slip-weakening rupture instability in landslides by localized increase of pore pressure. *Journal of Geophysical Research: Solid Earth*, *117*(B3).

Wallace, L. M., Webb, S. C., Ito, Y., Mochizuki, K., Hino, R., Henrys, S., … Sheehan, A. F. (2016). Slow slip near the trench at the hikurangi subduction zone, new zealand. *Science*, *352*(6286), 701–704.

Walter, J. I., Brodsky, E. E., Tulaczyk, S., Schwartz, S. Y., & Pettersson, R. (2011). Transient slip events from near-field seismic and geodetic data on a glacier fault, Whillans Ice Plain, West Antarctica. *Journal of Geophysical Research: Earth Surface*, *116*(F1).

Winberry, J. P., Anandakrishnan, S., Wiens, D. A., Alley, R. B., & Christianson, K. (2011). Dynamics of stick–slip motion, whillans ice stream, antarctica. *Earth and Planetary Science Letters*, *305*(3-4), 283–289.